5

Liquid Mixing in Agitated Vessels

To express the degree of mixing in a stirred vessel, an expression is desirable to show how far the state of mixing deviates from the ideal complete mixing. The most simple and popular index used in mixing studies is so called **mixing time**. Figure 5.0-1 shows the process of mixing in a stirred vessel. The termination point of this tracer experiment was taken when the reponse curve has reached

$$\frac{C(t)-C_\infty}{C_o-C_\infty}\times 100\% \le 5\% \qquad (5.0\text{-}1)$$

where C_∞, C_o, and C(t) are tracer concentration as the detected point at equilibrium, t=0 and time t respectively. The time needs to reach the termination state is known as "**mixing time** " of the system under the given condition as shown as t_M in Fig. 5.0-1 .

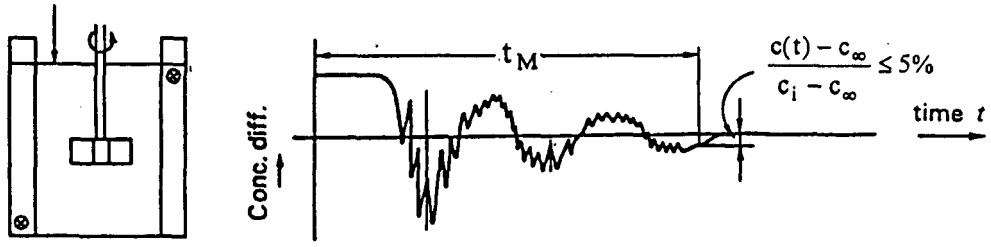

Fig. 5.0-1 Process of mixing and definition of mixing

The role of baffles in a mechanically agitated vessel is to prevent swirling and vortexing of liquid and to stabilize the power drawn by the impeller, thus greatly improving the mixing of liquid. By extending Nagata's (1975) work, Nishikawa et al.(1979) presented a relationship between the number of baffles and mixing time for single paddle impellers with four and six blades. They also defined the product of mixing time and power drawn by the impeller as **mixing energy** as an index to characterize the mixing in a mechanically agitated vessel. From their results, Nishikawa et al.(1979) pointed out that if the width of the baffle is larger than 0.1T, the fully baffled condition can be obtained if the number of baffle plates exceeds 3.

Sano and Hiromoto(1987) have studied the relationship between circulation rate and mixing time for various paddle impellers and have related the mixing time with the other operation variables as

$$Nt_M=(Nt_M)_{F.B.}/(1-0.62e^{-6.8\alpha}) \qquad (5.0\text{-}2)$$

where $\alpha=n_bB/T$ and $(Nt_M)_{F.B.C}=2.3(D/T)^{-1.67}(w/T)^{-0.74}n_P^{-0.47}$

Pandit and Joshi(1982), extending the model proposed by Joshi et al(1982) estimated the mixing time of the gassed stirred tank and obtained the following equation to predict mixing time in a gaased agitatated vessel.

$$Nt_M = 20.41\left(\frac{aH+T}{T}\right)\left(\frac{T}{D}\right)^{13/6}\left(\frac{W}{D}\right)\left(\frac{Q_S}{NV}\right)^{1/12}\left(\frac{N^2D^4}{gWV^{2/3}}\right)^{1/15} \qquad (5.0\text{-}3)$$

where the constant "a" depended on the size of the circulation loop and was equal to 1 for a centrally located impeller.

Nagase and Hiroo(1983) used the conductivity method to investigate the effect of gassing on the mixing efficiency of the mixing vessels with single vaned disc turbine and disc turbine. They found that under gassing , the mixing rate was reduced by 20% for the disc turbine and by 30% for the vaned disc turbine at low gas flow rates compared with ungassed conditions.

In retrospect, it can be seen that little research has been done for the effect of baffle design on mixing time in the stirred tank with Rushton impeller under gassing condition in the previous works. In this chapter, a study using both tracer technique and computer fluid dynamic approach to discuss how the baffle width, baffle number, rotational speed, gassing rate and impeller number will affect the extent of liquid mixing in a mechanically agitated vessel with Rushton turbine impeller.

5.1 Determination of Mixing Time for a Given System by Simulation

To determine the mixing time under extreme baffle conditions, several rotational speeds and the mixing time for multiple impellers systems, a numerical simulation program was devised to estimate the mixing time of the system with and without gassing. The commercially available computer software "Fluent" was used to simulate the single phase flow field of the individual agitated system. During the simulation, the impeller was always confined in a black box and the boundary conditions were set on the edges of this box. The boundary conditions including the kinetic energy, radial velocity, tangential velocity and vertical velocity were set after the LDA (Laser Doppler Anemometer) measurements, however the energy dissipasion rate was estimated from an expression proposed by Wu and Patterson (1989) ($\varepsilon=A\kappa^{3/2}/L_{res}$). The κ - ε turbulent model was adopted to determined the Reynolds stresses. Once the single phase flow field be detennined, the liquid velocity with gassing can be calculated from the results of Bakker and Van der Akker(1994) as follows:

$$U_{l,g}=U_{l,u}\times(P_g/P_o)^{\beta} \quad (5.1\text{-}1)$$

where $U_{l,g}$ and $U_{l,u}$ are the liquid phase velocity with and without gassing, P_g and P_o are the power consumption with and without gassing respectively. Then, the liquid volumetric flow rate can be calculated as follows:

$$q_{i,l,g}=U_{l,g}\times(areai,pro)\times(1-\varepsilon_g)^{\beta} \quad (5.1\text{-}2)$$

where $q_{i,l,g}$ was the liquid volumetric flow rate between cells in the i direction, $aera_{i,pro}$ is the projective area to the t direction and ε_g is the value of local gas hold-up which are obtained from the experimental dat of Jian(1992) and Lin(1994). By using the numerical simulation program, the mixing time of the system under gassed and ungassed conditions can be estimated and the most suitable exponent "β' was found to be 1 by comparing the simulated mixing time with the expenmental value.The procedures of this simulation is depicted in Fig.5.l-1 and the details can be found in Wu's thesis(1996).

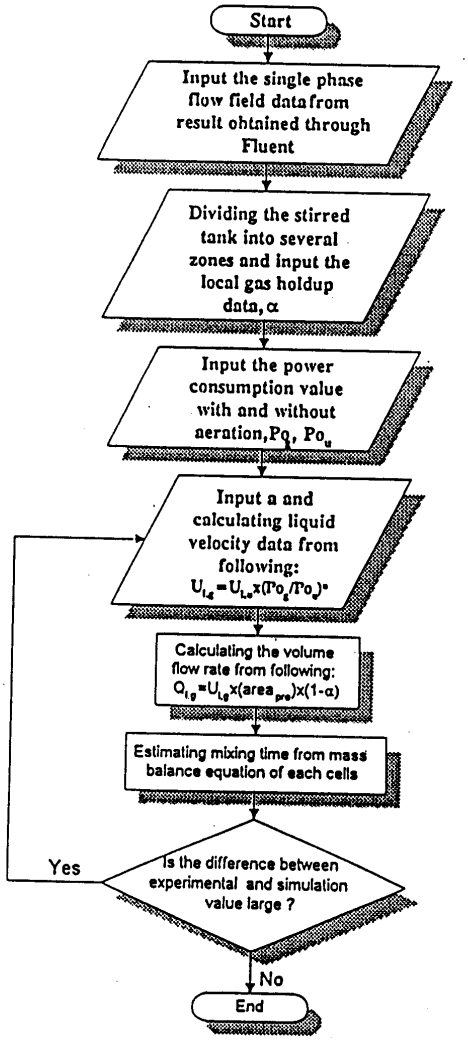

Fig. 5.1-1 The flow diagram of the simulated procedure for estimating the mixing time in gas-liquid agitated vessel.

Table 5.1-1 compares the simulated results with the experimental data, from which it can be seen that the simulation results can agree with the experimental data within a range of 10% deviation under gassed and ungassed conditions.

Table 5.1-1 Comparison of mixing time (t_M) between experimental and simulated methods.

Single Impeller System n_b=2 Q_g= 0L/min	Baffle Width / Mixing Time	0.05T	0.075T	0.1T	0.15T	0.2T
	Experimental data (sec)	14.6	13.7	13.0	12.1	11.5
	simulated data (sec)	14.8	14.2	13.4	12.0	11.7
	deviation (%)	1.30	3.60	3.00	0.83	1.74

5.2 Effect of Baffle Design on Mixing in Single Impeller System without Aeration

Figure 5.2-1 shows how the width and the number of baffle affect the extent of liquid mixing of the single impeller system under ungassed conditions for N=3.33rps in term of "mixing time". The results clearly indicate that insertion of baffles in the system can greatly improve the liquid mixing even when the ratio of B/T is less than 0.05. However, the fully baffled condition is difficult to achieve if the baffle number is less than three, which can be seen from the continuous decay curves for n_b= 2 and 3 in this figure. This result is different from what was observed by Nishikawa et al.(1979) for paddle impeller system which states that if $n_b \geqq 2$, the fully baffled condition can be obtained. In the systems for which the baffle number is more than four, the mixing time decreases steeply with the increase of the width of the baffle first, then it soon reaches a constant value as B/T exceeds 0.1. It is interesting to note that this leveling off value tends to decrease as the number of baffles increases in the range of n_b< 8 and B/T< 0.20. This fact implies that within this range, the increase of n_b and B/T will improve the extent of liquid mixing. However. the simulated results as shown in the figure by dotted lines also point out that the quality of liquid mixing will become worse if n_b is more than eight or B/T is larger than 0.25. The trend of growing worse in mixing is due to the localizing effect of excessive baffling. If the same plots are drawn for N= 5 and 6.67rps, it will be found that the trends of mixing tune are very similar to Fig.5.2-1. However the continuous decay of the mixing time with the increase of baffle width still exists for n_b=4 and the mixing time does not reach a leveling off value until B/T>0.15 and $n_b \geq 6$. Figure 5.2-2 shows the relationship between the mixing time and baffle width for n_b = 4 under various rotational speeds. It clearly indicates that (1)the increase of rotational speed will increase the liquid pumping capacity of the impeller thus the mixing quality will be improved;(2) the continuous decay trend of mixing time with the increase of baffle width becomes more

evident for larger rotational speeds and (3) the leveling off value of mixing time can be seen only for N=3.33rps, implying that it will be more difficult to attend the fully baffled condition if the rotational speed is higher. This phenomenon is consistent with the experimental results of the fully baffled condition for various rotational speeds obtained by the authors which indicate that the fully baffled condition for N=3.33, 5, 6.67rps are $n_b(B / T)^{1.2}$ =0.45, $n_b(B / T)^{1.2}$ = 0.67 and $n_b(B / T)^{1.2}$ =0.74 respectively (Lu et al. 1997)

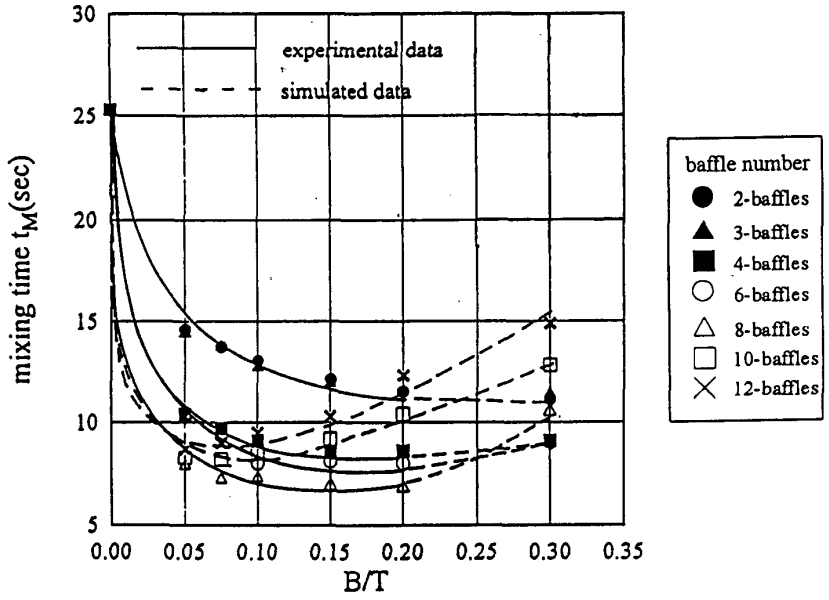

Fig. 5.2-1 Effect of baffle width on t_M for various number of baffles under ungassed condition for single impeller system with N=3.33rps.

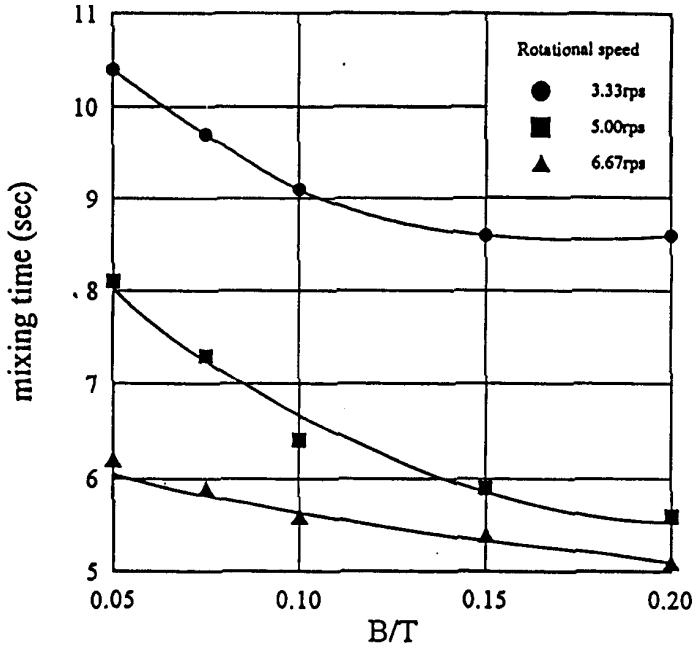

Fig. 5.2-2 Effect of baffle width on t_M with n_b=4 for various rotational speeds under ungassed condition.

To examine how the **mixing energy** (P_bt_M) is affected by the increase of baffle width and number, the plots of P_bt_m against B/T for various n_b with N=3.33rps are shown in Fig.5.2-3. The trend of these plots is very similar to what is seen in Fig.5.2-1. The value of mixing energy decreases first and soon reaches a leveling off value for a given number of baffles, except for $n_b \leqq 3$. In Fig.5.2-4, the same sets of data are also plotted into the other coordinates to examine how the mixing energy would vary with the number of baffles. The plots seem to indicate that the mixing energy decreases steeply with the increase of n_b by following almost the same path and then tends to converge into a constant value as n_b is larger than ten.

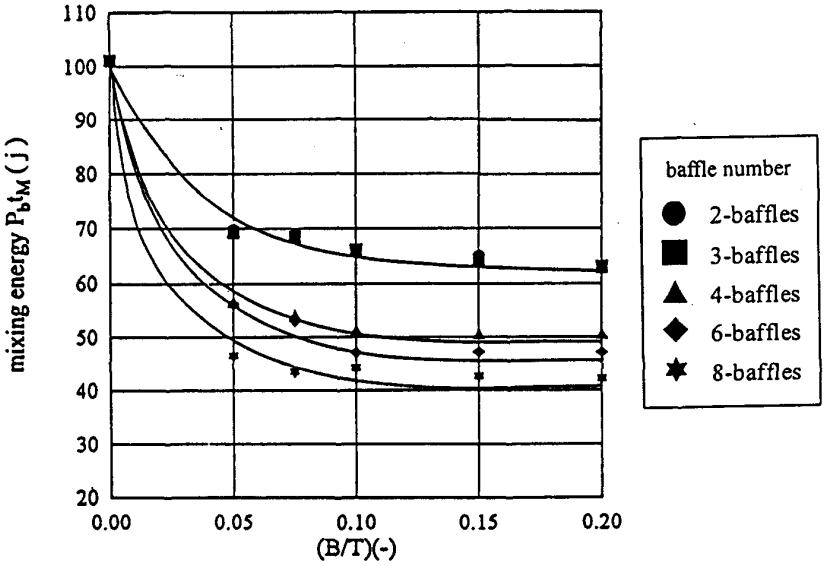

Fig. 5.2-3 Effect of baffle width on P_bt_M for single impeller system with various number of baffles under ungassed condition with N=3.33rps.

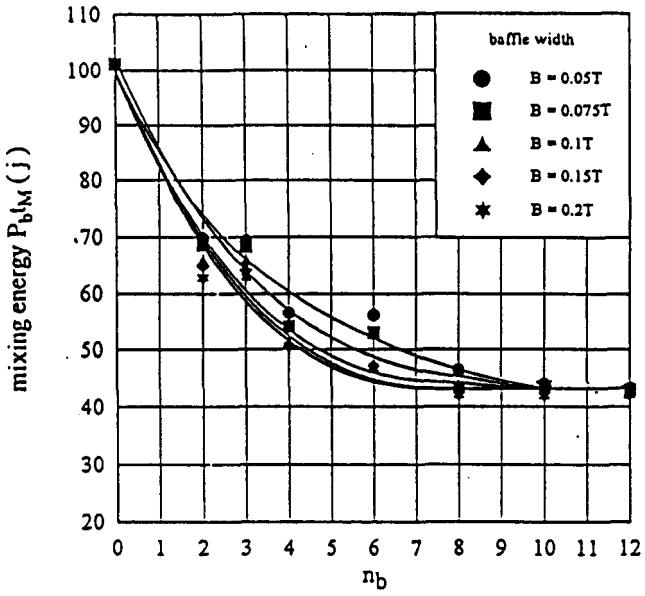

Fig. 5.2-4 Effect of baffle number on P_bt_M for single impeller system with various width of baffles under ungassed condition with N=3.33rps.

5.3 Effect of Baffle Design on Mixing in Single Impeller System with Aeration

To see how the effect of aeration will affect the quality of mixing, the mixing time under various aeration rates were determined and plotted in Fig.5.3-1 under N=3.33rps. It shows that the relationship between the mixing time and aeration rate for the system with B=0.15T for various baffle numbers. From this figure, it can be found that the increase in gassing rate would interrupt the liquid mixing to some extent, i.e. the mixing time will increase with the gassing rate at a lower gas flow rate region and reach a leveling off value as the gas flow rate exceeds 4 L/min which indicates that the impeller was flooded under this aerated rate. In order to examine the effect of the rotational speed on the relationship between mixing time and gassing rate, t_M vs. Q_S are plotted in Fig.5.3-2 for the case of n_b=4 and B/T=0.1 under various rotational speeds. The similar trends in mixing time can be observed for 5 and 6.67 rps in this figure. However the leveling off value of mixing time for 5 and 6.67rps will increase to higher aerated rates, i.e. about 9 and 17 L/min respectively under the same baffle conditions. Although the impeller becomes flooded, the impeller can still pump considerable amount of fluid in radial direction, thus the mixing quality will not be affected by the gassing rate under this circumstance

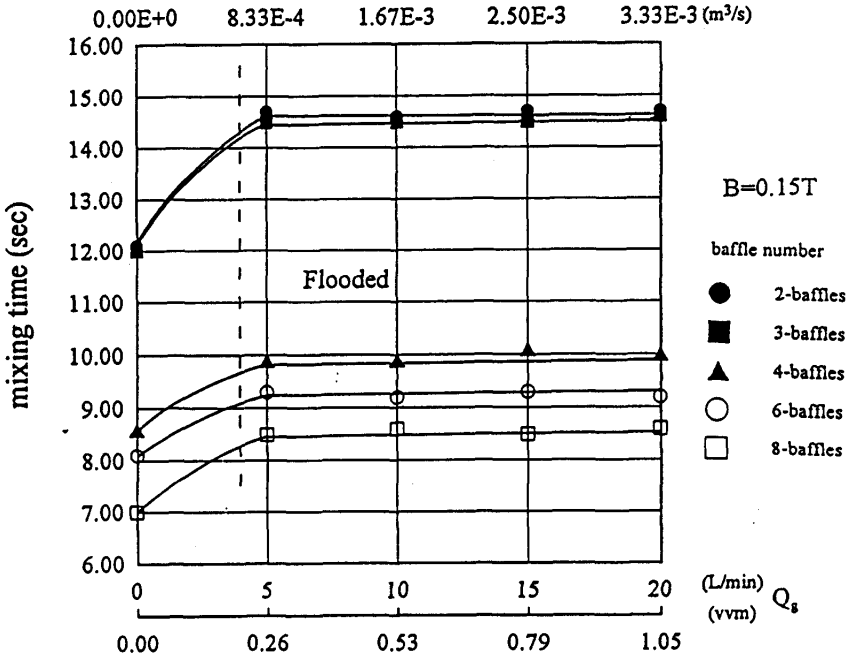

Fig. 5.3-1 Effect of gas flow rates on t_M for single impeller system with various width of baffles and N=3.33rps.

From these results, it can be said that if the impeller become flooded, the mixing time will be independent of aeration rate. The comparison of the flooding gassing rate for various rotational speeds between this study and the calculated values of the Greaves and Kobbacy's

(1981) correlation $N_F=152(T^{0.2}Q_S^{0.29}/D^{1.74})$ is also shown in Fig.5.3-2 for comparison. From this figure, it can be found that they agree very well with each other and the difference of flooding gassing rates for various rotational speeds between them is less than 20%.

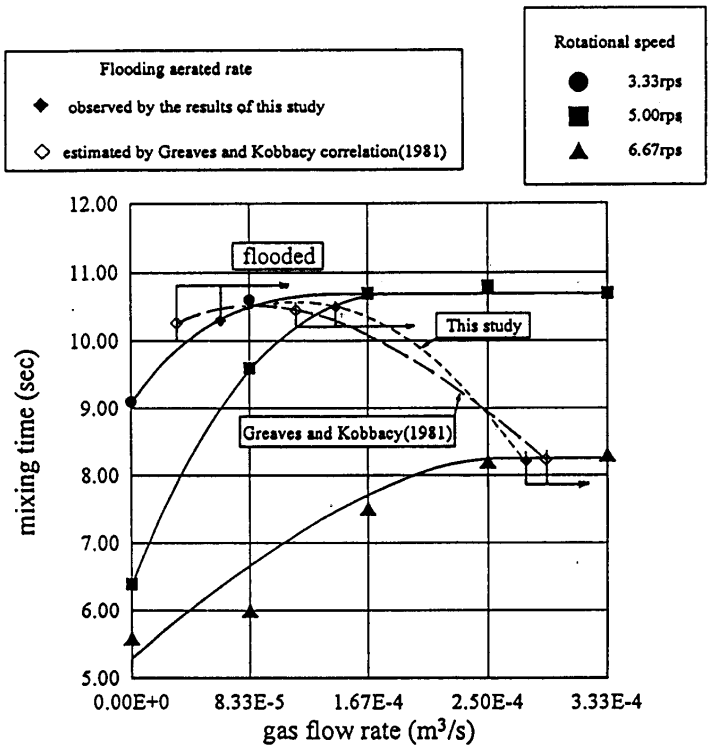

Fig. 5.3-2 Effect of gas flow rate on t_M for single impeller system with n_b=4 and B=0.1T under various rotational speeds and the comparison of the flooding aerated rate between this study and other correlation.

5.4 Effect of Baffle Design on Mixing in Multiple Impeller System

To see the relationship between mixing time and gas flow rate in a multiple impeller system, the simulated mixing time were plotted vs. gas flow rate for the systems equipped with dual and triple impellers with n_b=4, B/T=0.15 and N=3.33rps. It could be found that no matter what how many stages of impeller was, the trends of the mixing time are all similar, which always increases with the gassing rate initially then it reaches a level off value as the gas flow rate exceed a certain value. Once the gassing rate were larger than this value, all the impellers become flooded and the mixing time would be independent of gas flow rate. From Fig.5.4-1, it can be found that the flooded gas flow rates for the systems equipped with single, dual and triple impellers were 4L/min, 9L/min and 14L/min respectively. This difference is mainly due to the different gas loading of each impeller in the multiple impeller systems. Lu and Yao(1991) pointed out that only 30-40% of original feed gas flow through the upper impeller, thus the multiple impeller system could afford a large gassing rate than that the single impeller system before it became flood.

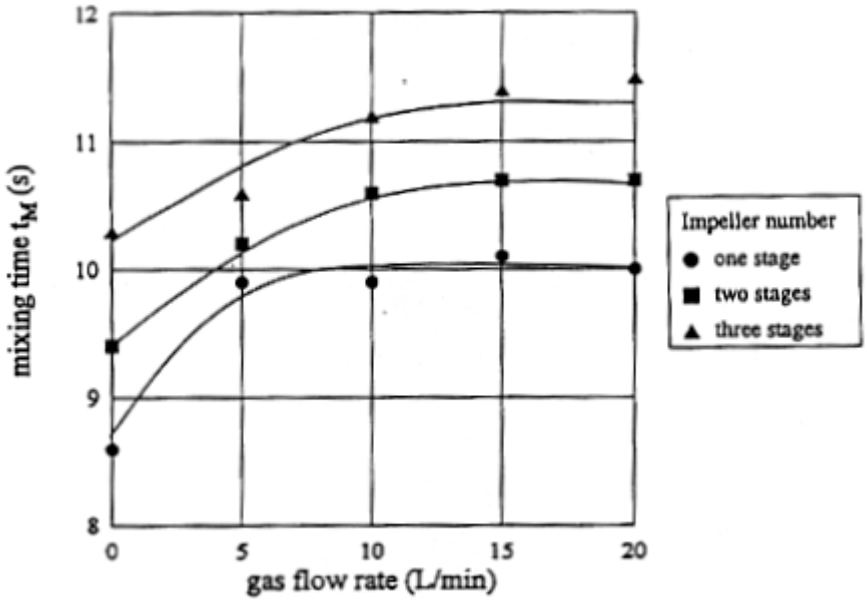

Fig. 5.4-1 Effect of impeller on the relationship between t_M and Q_S with N=3.33rps.

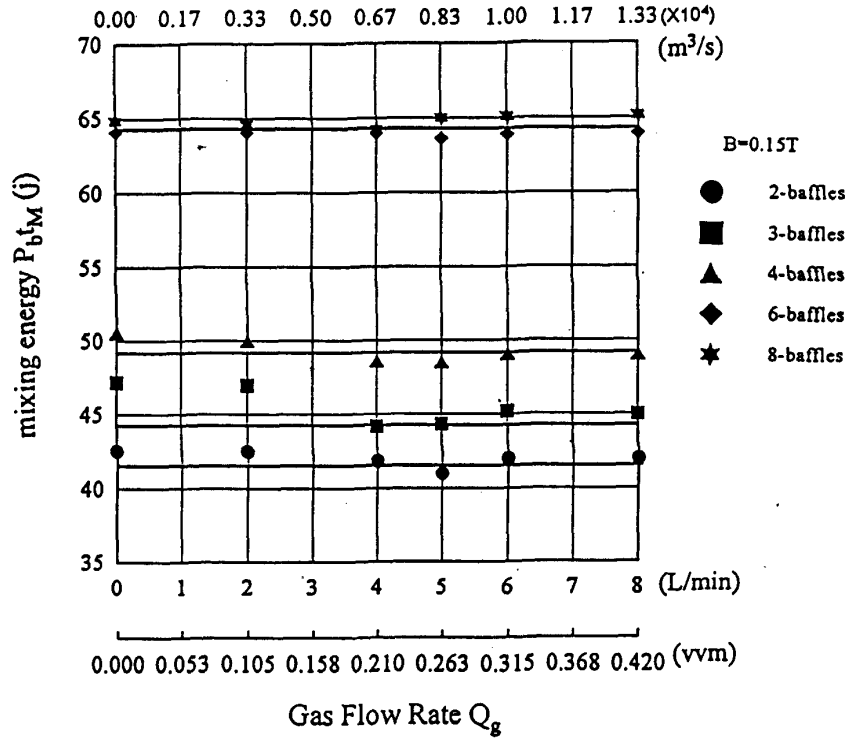

Fig. 5.4-2 Effect of gas flow rate on P_bt_M for single impeller system with various width of baffles under N=3.33rps.

When the same sets of data are replotted as P_bt_M against Q_S with various n_b for a given B/T as shown in Fig.5.4-2, the plots show that the gas flow rate has no effect on mixing energy while it interrupts the liquid mixing as seen in Fig.5.4-1. This implies that the mixing energy itself can not be served as a sole basis to judge the fully baffled condition for a given system. From the above results, it seems to imply that the mixing time decreases with the

increasing of the power consumption. In order to confirm this point, P_g for various gas flow rates are plotted against t_M as shown in Fig.5.4-3. From these plots, it can be found that no matter what values of Q_S or a given n_b, the trends between P_g and t_M are all similar which implies that the mixing quality will be improved as P_g increases. However, for a given Q_S, if the number of the baffle is increased from 4 to 6, a slight inverse trend will be observed which is the results of the contradict between the effects of hindrance and localizing phenomenon of baffles. The hindrance effect of baffles increases the power consumption and the turbulence in the vessel (i.e. decrease t_M). However, the localizing phenomenon behind baffles not only reduces the fluid loading of impeller which causes the decreasing of P_g, but also diminishes the interaction between baffle regions which makes mixing quality becomes worse.

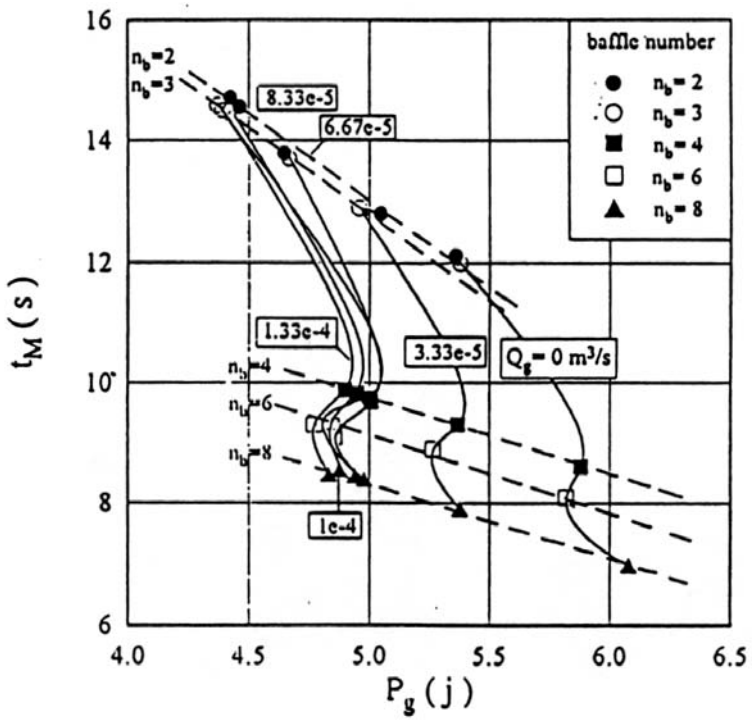

Fig. 5.4-3 The relationship between P_g and t_M with various gas flow rates and baffle number with B=0.15T.

For the systems with dual and triple impellers, the relationships between t_M and width or number of the baffle are very similar to those of the single impeller system and they are summarized and compared with the single impeller system in Table 5.4-1. From the data shown in this table, it can be seen that the values of mixing time always increase with the increase of impeller number and the difference between them becomes smaller as the baffle width become larger. It is also interesting to notice that this difference increases almost double as it reaches the fully baffled condition if it is compared with the case of n_b, is 2 or 3.

Table 5.4-1 Comparison of mixing two between the single and triple impeller systems.

	Baffle Width / Mixing Time (s)	0.05T	0.075T	0.1T	0.15T	0.2T
n_b=2	Single Impeller System(Ⅰ)	14.6	13.7	13.0	12.1	11.5
	Triple Impeller system (Ⅱ)	18.6	16.2	14.5	13.3	12.6
	Difference(Ⅱ/Ⅰ)×100%	27.4	18.2	11.5	9.92	9.57
n_b=3	Baffle Width / Mixing Time (s)	0.05T	0.075T	0.1T	0.15T	0.2T
	Single Impeller System(Ⅰ)	14.5	13.8	12.8	12.0	11.6
	Triple Impeller system (Ⅱ)	18.7	16.3	14.4	13.2	12.6
	Difference(Ⅱ/Ⅰ)×100%	29.0	18.1	12.5	10.0	8.62
n_b=4	Baffle Width / Mixing Time (s)	0.05T	0.075T	0.1T	0.15T	0.2T
	Single Impeller System(Ⅰ)	10.4	9.7	9.1	8.6	8.6
	Triple Impeller system (Ⅱ)	1635	14.1	12.0	10.3	9.7
	Difference(Ⅱ/Ⅰ)×100%	58.7	45.4	31.9	19.8	12.8
n_b=6	Baffle Width / Mixing Time (s)	0.05T	0.075T	0.1T	0.15T	0.2T
	Single Impeller System(Ⅰ)	10.3	9.3	8.0	8.1	8.0
	Triple Impeller system (Ⅱ)	14.8	13.2	10.5	9.0	9.0
	Difference(Ⅱ/Ⅰ)×100%	43.7	41.9	31.3	11.1	12.5
n_b=8	Baffle Width / Mixing Time (s)	0.05T	0.075T	0.1T	0.15T	0.2T
	Single Impeller System(Ⅰ)	7.9	7.2	7.3	7.0	6.9
	Triple Impeller system (Ⅱ)	13.4	11.4	8.7	8.4	8.3
	Difference(Ⅱ/Ⅰ)×100%	69.6	58.3	19.2	20.0	20.3

5.5 Equations to Predict Mixing Time

To obtain a more comprehensive and reliable relationship for the operating parameters, the mixing time data obtained experimentally and numerically are correlated with n_b and B/T and Q_S under various rotational speeds and a dimensionless correlation can be given as:

$$Nt_M=55.7(n_b)^{-0.30}(B/T)^{-0.1535}(Q_S/ND^3)^{0.0296} \qquad (5.5\text{-}1)$$

for the single Rushton impeller system. If the simulated value of mixing time for dual and triple impeller systems are correlated with the same parameters as the the single impeller system, then the similar correlations for the dual and triple impeller systems can be given as:

For dual impeller system $$Nt_M=50.3(n_b)^{-0.298}(B/T)^{-0.253}(Q_S/ND^3)^{0.021} \qquad (5.5\text{-}2)$$

For triple impeller system $$Nt_M=46.5(n_b)^{-0.295}(B/T)^{-0.327}(Q_S/ND^3)^{0.010} \qquad (5.5\text{-}3)$$

respectively. The standard deviation of these three above equations are all smaller than 20%. From these three equations, it can be seen that the dimensionless mixing time decreases with the increase of n_b, B/T and N, however it increases as Q_S increases. The effect of baffle number on mixing time is more pronounced than baffle width in the single impeller system, however the gradually inverse situations are found in the dual and triple impeller systems. From these three equations it may be misunderstood that the effect of gas flow rate on mixing

time is small, however if the dimensional groups are used, the above three empirical equations can be rewritten as:

$$Nt_M=32.4(n_b)^{-0.275}(B/T)^{-0.140}(Q_S)^{0.208} \quad (5.5\text{-}4)$$

$$Nt_M=32.1(n_b)^{-0.283}(B/T)^{-0.271}(Q_S)^{0.196} \quad (5.5\text{-}5)$$

$$Nt_M=31.1(n_b)^{-0.289}(B/T)^{-0.320}(Q_S)^{0.171} \quad (5.5\text{-}6)$$

which look more reasonable than the original dimensionless equations. Once the impeller number was adopted as another variable, then Eqns.(5.5-1), (5.5-2) and (5.5-3) can be combined and rewritten into the following single correlation.

$$Nt_M=42.7(n_b)^{-0.308}(B/T)^{-0.237}(n_I)^{0.316}(Q_S/ND^3)^{0.0181} \quad (5.5\text{-}7)$$

The deviation of this correlation was within 25% and the final results was depicted in Fig.5.5-1. With this empirical equation the mixing quality tinder a given operating condition can be predicted for the systems equipped with Rushton impellers.

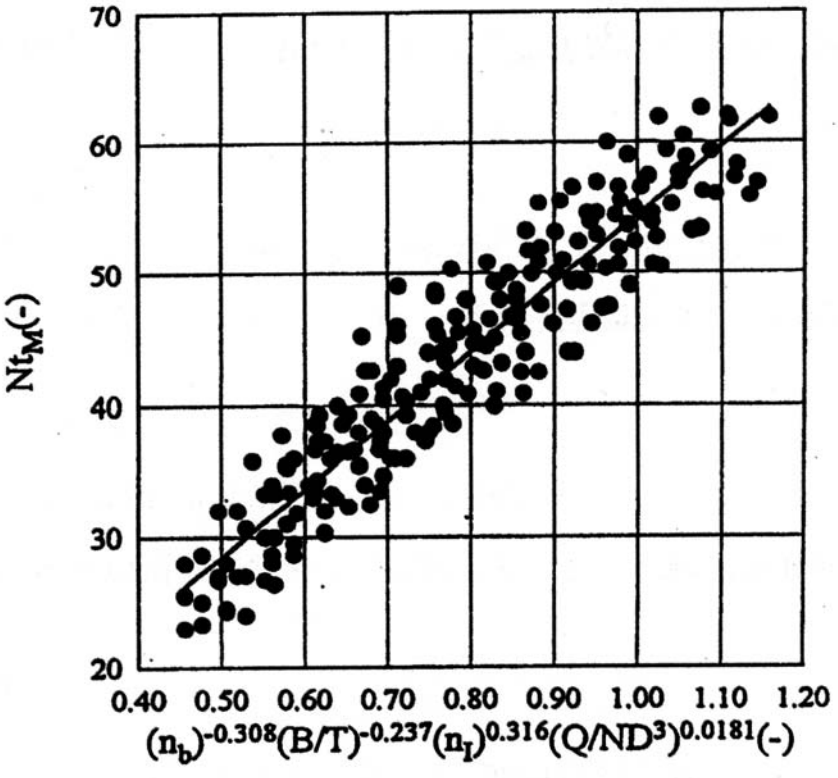

Fig. 5.5-1 The regressive results of the final empirical equation.

5.6 Non-Uniformity within the Gassed Stirred Vessels

Since the distribution of mixing intensity exerts a great impact to the product yield and can be used as a criterion for design an agitated gas-liquid reactor, many researchers had dedicated to the mixing strength within an agitated system. However, most of them only discussed the mixing intensity through the relevant characteristics based on the macroscopic phenomena, such as mixing time, mass transfer coefficient and power demand, etc. Even

though the mean turbulent intensity in a stirred vessel was discussed in author's previous works (Lu and Wang, 1986; Lu and Chen, 1986; Lu and Wu, 1988; Lu and Ju, 1996), no local distribution of turbulent intensity, which is related to the mixing intensity, was considered, especially for the gassed agitated system. By extending the probability theories of solid mixing to the liquid-liquid systems, Ogawa and Ito (1975) defined a new index to identify the quality of mixing by making use of the information entropy, and the results were applied to the batch and steady flow systems. Ogawa et al. (1980) compared the mixing capabilities of various impeller types using the mixing index defined by Ogawa and Ito (1975). They found there was a basic relationship between the quality of mixing and dimensionless mixing time N_t, and the impellers with different types give only different proportional coefficients. Ogawa (1982) defined new local and overall mixing capacity indices based on the concept of information entropy to discuss the distribution of mixing intensity within various single impeller systems. In this study, the **mixing capacity index** defined by Ogawa (1982) were adopted to gassed single and multiple impeller systems to examine how the gassing rate and rotational speed will affect the mixing intensity in the agitated systems. Distributions of local mixing capacity index, I_L for different impeller combinations were also evaluated to examine the effects of the gas dispersion capability of the impeller and the strength of liquid flow on the mixing efficiency.

5.6.1 Theories of the mixing capacity indices

Assume the transition probability, A_{ij}, that the liquid involved in region i enter region j as shown in Fig. 5.6.1-1 in unit time Δt is known. The transition is considered to be complete when the liquid at all points in region i enters all of points in region j with the same probability and is independent of the transitional path.

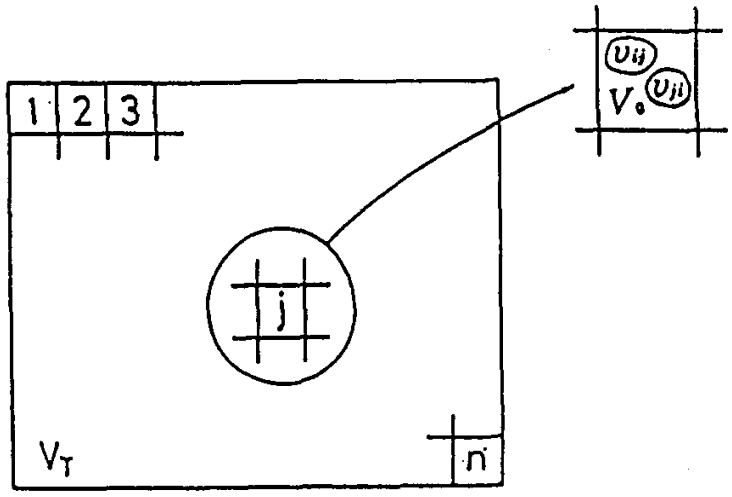

Fig. 5.6.1-1 Mixing of the fluid elements.

1. Local mixing capacity index

Liquid transports with respect to region *i* are divided into two parts, i.e. inflow and outflow. The transitional probability, a_{ij}, which denotes the liquid involved in region *i* enter region *j* of the characteristic volume V_O in unit time Δt, can be rewritten as follows:

$$a_{ij} = A_{ij} \frac{V_O}{V_j} \tag{5.6.1-1}$$

The amount of information associated with the news, which informs the liquid involved in region *i* enter region *j* of the characteristic volume V_O in unit time Δt, can be expressed as *-log* a_{ij} and the probability that this news is transmitted in $(V_j/V_O)a_{ij}$ according to the information theory. Therefore, when no news concerning the region into which the noticed liquid element goes is transmitted, the average amount of information per the news is expected.

$$H_{O,1} = -\sum_{j=1}^{n} \frac{V_j}{V_O} a_{ij} \log a_{ij} \tag{5.6.1-2}$$

This average amount of information shows the amount of uncertainty, which is held before the result concerning the region into which the liquid element outflow is transmitted. After the news concerning the result is transmitted, the amount of uncertainty concerning the result becomes zero, that is to say, the amount of information associated with the news, which informs the region into which the liquid element outflow is expressed as:

$$I_{O,1} = H_{O,1} - 0 = -\sum_{j=1}^{n} \frac{V_j}{V_O} a_{ij} \log a_{ij} \tag{5.6.1-3}$$

In a much similar way, the average amount of information associated with the news, which informs the region into which the liquid element inflow can be presented as:

$$I_{I,i} = -\sum_{j=1}^{n} \frac{V_j}{V_O} a_{ji} \log a_{ji} \tag{5.6.1-4}$$

As for the region *i*, from the viewpoint of mixing capacity, the exchange of liquid with more regions with more equal probability is better than that with restricted regions with partial probability, that is to say, the higher degree of the uncertainties described above shows a higher mixing capacity. Assuming that the weight of outflow and inflow on the local mixing capacity are the same, the mean value of $I_{O,I}$ and $I_{I,i}$ represents the amount of local mixing entropy of region *i* as:

$$I_i = \frac{1}{2}(I_{O,1} + I_{I,i}) = -\frac{1}{2}\sum_{j=1}^{n} \frac{V_j}{V_O}(\mathrm{a_{ij}} \log a_{ij} + a_{ji} \log a_{ji}) \tag{5.6.1-5}$$

It is clear mathematically that this local mixing entropy takes the minimum and the maximum

values as follows, respectively.

$$I_{i,\min} = 0 \qquad \text{at } a_{ij}=1 \text{ or } 0 \qquad (A_{ij}=V_j/V_O \text{ or } 0) \tag{5.6.1-6}$$

$$I_{i,\max} = -\log\frac{V_O}{V_T} \quad \text{at } a_{ij}=V_O/V_T \qquad (A_{ij}=V_j/V_T) \tag{5.6.1-7}$$

The conditions described above were consistent with the statements at which the liquid in region *i* is not mixed at all with the liquids in other regions and at which the liquid in region *i* is mixed completely with the liquid in other regions, respectively. Considering that the general stirring status lies between these two extreme conditions described above, the local mixing capacity index can be defined as follows:

$$I_{L,i} = \frac{I_i - I_{i,\min}}{I_{i,\max} - I_{i,\min}} = -\frac{1}{2}\frac{\sum_{j=1}^{n}\frac{V_j}{V_O}(\mathrm{a_{ij}}\log a_{ij} + a_{ji}\log a_{ji})}{\log(V_O/V_T)} \tag{5.6.1-8}$$

In accordance with the above definition, it is aware that the local mixing capacity index varies from *0* for complete segregation to *1* for complete mixing.

2. Overall mixing capacity index

The overall mixing entropy can be defined as the average of the local mixing entropy weighted in accordance with the probability $P_{V,i}(=V_i/V_T)$ as:

$$I_w = \sum_{i=1}^{n} P_{V,1} I_i = -\sum_{i=1}^{n}\sum_{j=1}^{n}\frac{1}{2}\frac{V_i V_j}{V_O V_T}(\mathrm{a_{ij}}\log a_{ij} + a_{ji}\log a_{ji}) \tag{5.6.1-9}$$

This overall mixing capacity entropy takes the same minimum and maximum values under identical conditions as those for the case of local mixing capacity entropy, I_i, and it is suitable to define the overall mixing capacity index as follows:

$$I_w = -\frac{1}{2}\frac{\sum_{i=1}^{n}\sum_{j=1}^{n}\frac{V_i V_j}{V_O V_T}(\mathrm{a_{ij}}\log a_{ij} + a_{ji}\log a_{ji})}{\log(V_O/V_T)} \tag{5.6.1-10}$$

Being analogous to the local mixing capacity index, the overall mixing capacity index change from zero for no mixing state to unity for complete mixing state. The detailed procedure for evaluating the values of I_L and I_W can be consulted in Ogawa (1982).

5.6.2 Distribution of local mixing capacity index

The local mixing capacity index, I_L for the single Rushton turbine impeller system under an ungassed condition with *N=3.33rps* was evaluated and the results are shown as a contour map in Fig. 5.6.2-1 along with the calculated flow pattern after *CFD* simulation (Lu et al, 2000a). The largest value of I_L always appears in the discharge stream of impeller close to

tank wall, where the discharged liquid flow changes its direction from radial to axial and splits into two liquid circulating loops, therefore, results in larger turbulent intensity and mixing intensity. With departing off the impeller discharge region, the turbulent intensity decreases, which causes the decreases in I_L along the liquid circulating loop and give weaker mixing intensities in the positions near the liquid surface and tank bottom. Comparing the contour maps of I_L at different *R-Z* planes as shown in Fig. 5.6.2-2, one can find that in the azimuthal planes near the baffle plate, the localization of maximum I_L in the discharge stream of impeller close to tank wall will be suppressed. This phenomenon is more obvious for the plane behind the baffle plate, which gives a more uniform distribution of I_L than those in the other two planes. According to Eq. 5.6.1-1, the overall mixing capacity index I_W for the single Rushton turbine impeller system with *N=3.33rps* under an ungassed condition was evaluated as *0.484*.

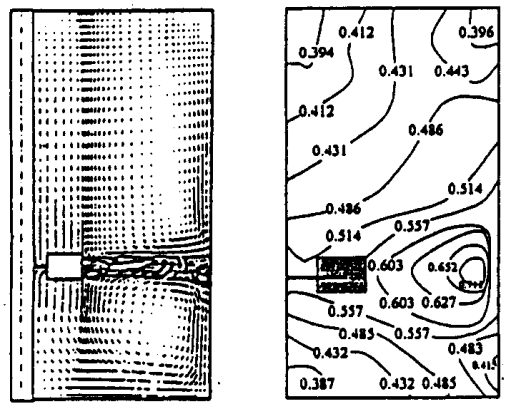

Fig. 5.6.2-1 Contour map of local mixing capacity index I_L in the mid-plane along with the flow pattern after Lu et al.(2000a) with *N=3.33rps* under an ungassed condition.

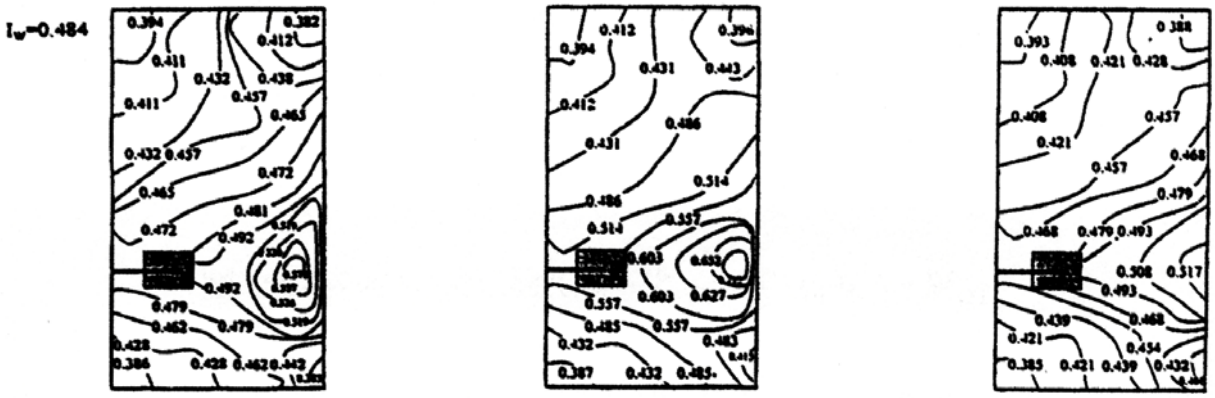

(a) θ= +10° (b) θ= 45° (c) θ= -10°

Fig. 5.6.2-2 Comparison of the contour maps of local mixing capacity index I_L in three different *R-Z* planes with *N=3.33rps* (a) in front of baffle; (b) mid-plane and (c) behind baffle.

Figure 5.6.2-3 shows the distributions of I_L in different *R-Z* planes for the triple Rushton turbine impeller system. The trends of I_L in this figure are very similar to what were seen in the single Rushton turbine impeller system. In other words, the largest values of I_L always appear in the discharge stream of each impeller close to tank wall and decay with departing off the impeller region, under which there are three localizations of maximum I_L. The distribution of I_L around each impeller region looks alike, which indicates the mixing intensity around each impeller is similar under an ungassed condition and each impeller can be deemed as independent with *C=2D*. The values of I_L in mid-plane are much higher than those in the other two planes, and the local maximum values of I_L in the discharge stream of each impeller will disappear as it close to the baffle plate. It is seen that although the larger mixing intensities still take place at the discharge stream of each impeller, the multiple impeller configuration is conducive to diminish this non-uniformity comparing to the single impeller system. The overall mixing capacity index I_W for the triple Rushton turbine impeller system is *0.615*, which is much larger than I_W*=0.514* for the single Rushton turbine impeller system. This fact implies that with a given *N* or P_g/V, the multiple impeller system can give not only a more uniform mixing intensity within the system, but also results in a higher overall mixing capacity than the single impeller system, which is beneficial for the process requirement.

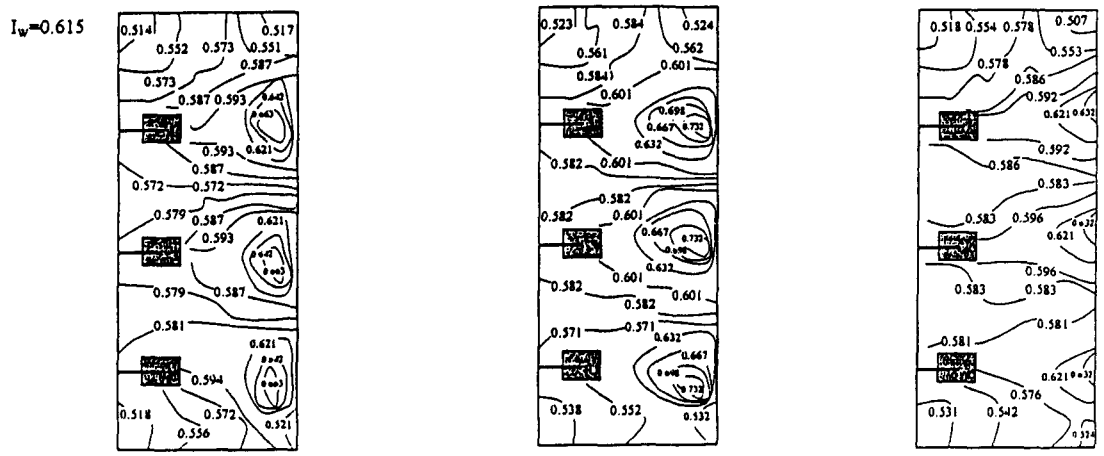

(a) θ= +10° (b) θ= 45° (c) θ= -10°

Fig. 5.6.2-3 The contour maps of local mixing capacity index I_L in various azimuthal planes for the triple Rushton turbine impeller system with *N=3.33rps* (a) in front of baffle; (b) mid-plane and (c) behind baffle.

5.6.3 Effect of aeration on the mixing intensity

To examine the effect of aeration rate on the mixing intensity within agitated systems, the local and overall mixing capacity indices for the systems with different aeration rates were determined based on the experimental data. Figure 5.6.3-1 shows the contour maps of local

mixing capacity index I_L in mid-plane for the single Rushton turbine impeller system with various gassing rates and $P_g/V=1004.4W/m^3$. The overall mixing capacity index I_W for each aeration rate was also calculated and listed in this figure for comparison. The position of the region with extremely larger I_L values shifts upward and becomes vaguer and vaguer with the increase in aeration rate due to the induced liquid flow given by the uprising gas. This fact indicates that aeration is helpful to eliminate the non-uniformity within the agitated system. Since aeration has a retarded effect on the liquid pumping rate of the impeller, which reduces the strength of the liquid circulating flow, the value of overall mixing capacity index I_W decreases with the increase in the aeration rate under a lower gassing rate condition. However, as the aeration rate exceeds a certain value, I_W increases with the increase in gassing rate, especially when the aeration rate makes the impeller flooded ($Q_S>0.75vvm$), under which the rising bubbles will enhance the circulation of liquid and results in a larger value of I_W.

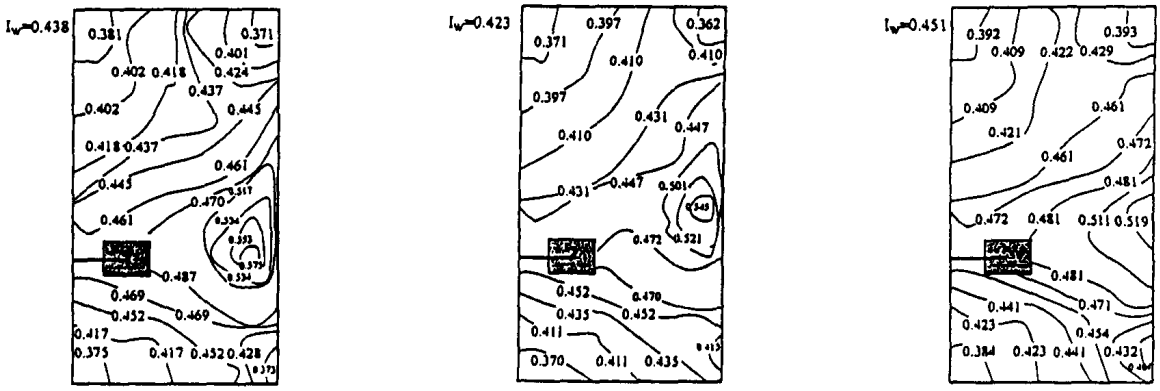

Fig. 5.6.3-1 The contour maps of local mixing capacity index I_L and the overall mixing index I_W for the single Rushton turbine impeller system under various aeration rates with $P_g/V=1004.4W/m^3$.

Figure 5.6.3-2 depicts the distributions of I_L in the mid-plane for the triple Rushton turbine impeller system with various aeration rates and $P_g/V=1004.4W/m^3$. Comparing the contour maps in this figure to those shown in Fig. 5.6.2-3, it can be seen that for the triple Rushton impeller system, the trend of shifting upward for the larger I_L region with the increase in aeration rate is less obvious. However, it is easier to suppress the regions of maximum I_L by increasing the aeration rate than that in the single Rushton turbine impeller system. The higher I_L core existed in the discharge stream of the lowest impeller is eliminated first, then the mixing intensity concentrated region for the middle impeller will be suppressed, and finally the larger I_L region for the upper impeller also disappear if the aeration rate is increased further. The triple Rushton impeller system gives not only a more uniform distribution of mixing intensity, but also a higher overall mixing capacity index than the

single Rushton impeller system, which is good for the volume utilization of a chemical reactor.

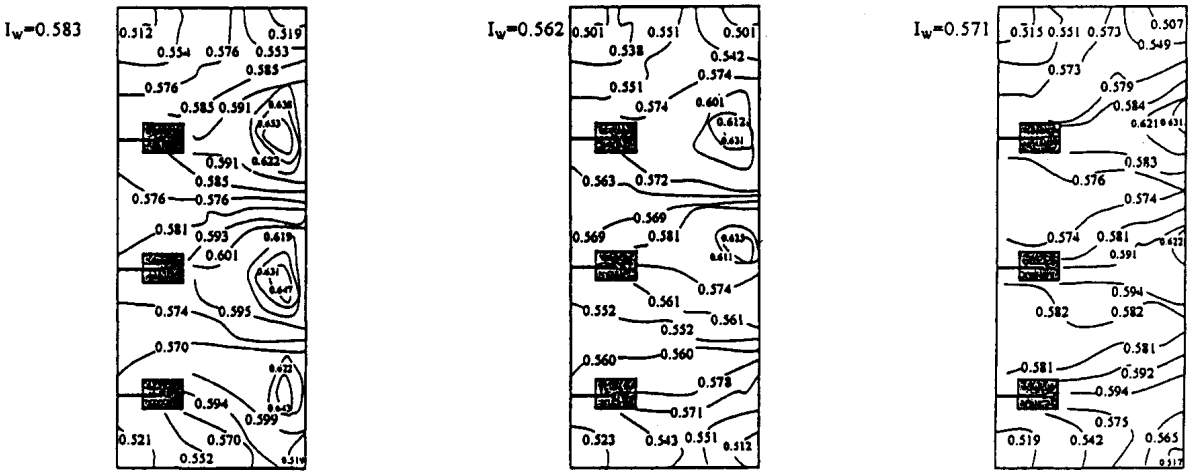

(a) Q_s= 0.22 vvm (b) Q_s= 0.52 vvm (d) Q_s= 0.78 vvm

Fig. 5.6.3-2 The contour maps of local mixing capacity index I_L and the overall mixing index I_W for the triple Rushton turbine impeller system under various aeration rates with P_g/V=1004.4W/m^3.

5.6.4 Effect of flow pattern on I_L distribution

As pointed out by Lu et al.(2000b), since the *PPR* system gives a stronger liquid circulating flow around the whole system, it results in a higher mass transfer rate than the *RRR* system. Therefore, it is worthwhile to examine whether the *PPR* system has a stronger mixing intensity than the *RRR* system or not. Figure 5.6.4-1 depicts the distributions of I_L and the values of I_W for these two systems with Q_S=0.52vvm and P_g/V=1004.4W/m^3. From the comparison of these two figures, one can find that: (1) a more homogeneous distribution of I_L was obtained for the *PPR* system; (2) due to the enforced flow from the upper two pitched blade impellers, the liquid pumping rate of the lower Rushton turbine impeller increases, which induces the localization of larger I_L appear in the discharge region of the lower Rushton turbine impeller comparing to the *RRR* system; (3) under a gas completely dispersed condition, the stronger liquid circulating flow produced by the *PPR* system not only suppresses the localization of larger I_L, but also results in a larger value of I_W.

5.6.5 Concluding remarks

Distributions of the local mixing capacity I_L illustrate that no matter for the single or multiple impeller systems, the mixing intensities are always the strongest in the discharge stream of each impeller close to tank wall. Comparing the contour plots in different azimuthal planes for various systems, it is found that the baffle plate as well as the multiple impeller configuration will suppress the local maximum values of I_L in the discharge stream of each

impeller, which is beneficial to the volume utilization of a reactor. Under a gassing condition, the position of the region with extremely larger I_L values shifts upward and becomes vaguer and vaguer with the increase in aeration rate, which indicates that aeration is helpful to eliminate the non-uniformity within the agitated system. The value of overall mixing capacity index I_W decreases with the increase in the aeration rate under a lower gassing rate condition, while it increases with the increase in gassing rate as the aeration rate is large enough to make the impeller flooded. Comparing the distributions of I_L in single and multiple impeller systems under various operating conditions, it can be concluded that the multiple impeller system not only gives a more uniform and higher mixing intensity, but also provides a higher gas utilization than the single impeller system. Once the gas is completely dispersed, the *PPR* impeller system will possess a better mixing efficiency than the *RRR* system with a given energy dissipation density.

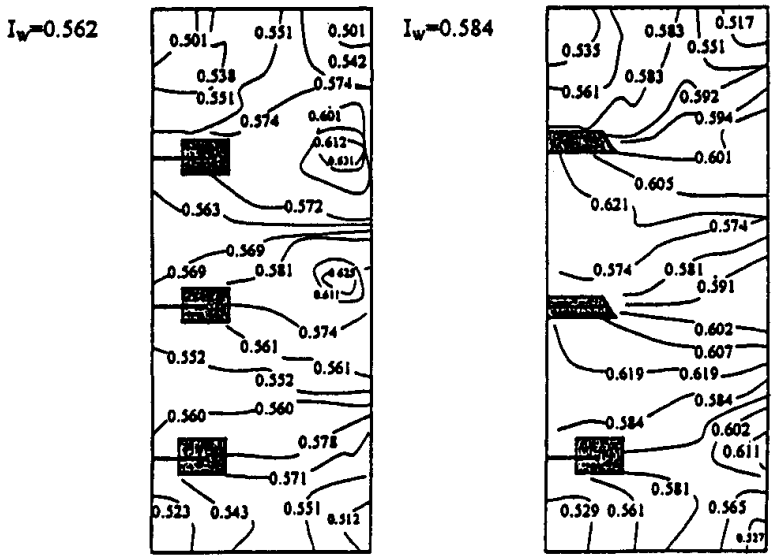

(a) RRR system (b) PRR system

Fig. 5.6.4-1 The contour maps of local mixing capacity index I_L and the overall mixing index I_W for the RRR and PPR impeller systems under various aeration rates with Q_S=0.52vvm and P_g/V=1004.4W/m^3.

NOTATION

a	Parameter in Eq.(5.0-3)	[-]
B	Baffle width	[m]
c	Tracer concentration	[M]
c(t)	Tracer concentration at time t	[M]
C	Distance between impellers	[m]

C_l	Height of lower impeller from bottom	[m]
D	Impeller diameter	[m]
H	Liquid level of stirred tank	[m]
L	Length of impeller blade	[m]
L_{res}	Resultant turbulence scale	[m]
N	Impeller rotational speed	[1/s]
n_b	Baffle number	[-]
n_I	Impeller number	[-]
n_p	Number of impeller blade	[-]
P_b	Power consumption with baffle	[kgm^2/s^3]
P_g	Power consumption with aeration	[kgm^2/s^3]
P_o	Power consumption without aeration	[kgm^2/s^3]
Q_s	Sparged gas flow rate	[m^3/s]
$q_{i,l,g}$	Liquid volumetric flow rate between cells in the I direction	[m^3/s]
T	Tank diameter	[m]
t_M	Mixing time	[s]
$U_{l,g}$	Liquid phase velocity with aeration	[m/s]
$U_{l,u}$	Liquid phase velocity without aeration	[m/s]
u',v'	Fluctuation velocity	[m/s]
V	Liquid volume in the tank	[m^3]
W	Mean tangential velocity	[m/s]
w	Impeller blade width	[m]

<*Greeks Letters*>

α	Defined in Eq.(6-1)($=n_bB/T$)	[-]
β	Exponent adopted in Eq.(5.1-2)	[-]
ε	Energy dispersion rate	[m^2/s^3]
ε_g	Local gas hold-up	[-]
θ	Shaft angular position	[degree]
κ	Turbulent kinetic energy	[m^2/s^2]

<*Subscripts*>

g	Gassed condition
i	Any principle direction
i	Initial condition
l	Liquid phase
Pro	Projective
u	Ungassed condition
∞	Final condition